ARTICLES

Electron Transfer in Porphyrin Complexes in Different Solvents

Dmitri Kilin, Ulrich Kleinekathöfer,* and Michael Schreiber

Institut für Physik, Technische Universität, D-09107 Chemnitz, Germany

Received: December 9, 1999; In Final Form: March 20, 2000

Electron transfer (ET) in different solvents is investigated for systems consisting of donor, bridge, and acceptor. It is assumed that vibrational relaxation is much faster than the ET. ET rates and final populations of the acceptor state are calculated numerically and in an approximate fashion analytically. In wide parameter regimes these solutions are in very good agreement. The theory is applied to the ET in $H_2P-ZnP-Q$, with free-base porphyrin (H_2P) being the donor, zinc porphyrin (ZnP) the bridge, and quinone (Q) the acceptor. It is shown that the ET rates can be controlled efficiently by changing the energy of the bridging level, which can be done by changing the solvent. The solvent effect is determined for different models. PACS numbers: 31.70.Hq, 34.70.+e, 82.20.Rp

I. Introduction

Electron transfer (ET) is a very important process in biology, chemistry, and physics.[1−5] The most well-known ET theory is the one of Marcus.[6] Of special interest is the ET in configurations where a bridge (B) between donor (D) and acceptor (A) mediates the transfer. On this kind of ET we will focus in this paper. The primary step of ET in bacterial photosynthetic reaction centers is of this type,[7] and a lot of work in this direction was done after the structure of the protein−pigment complex of the photosynthetic reaction centers of purple bacteria was clarified in 1984.[8] Many artificial systems, especially self-organized porphyrin complexes, have been developed to model this bacterial photosynthetic reaction center.[3,9,10]

Bridge-mediated ET reactions can occur via different mechanisms:[4,11−13] incoherent sequential transfer in which the bridge level is populated, or coherent superexchange[14,15] in which the mediating bridge level is not populated but nevertheless necessary for the transfer. Changing a building block of the complex[9,16,17] or changing the environment[16,18] can modify which mechanism is mainly at work. Actually, there is still a discussion in the literature as to whether sequential transfer and superexchange are limiting cases of one process[19] or whether they are two processes that can coexist.[7] To clarify which mechanism is present in an artificial system one can systematically vary the energetics of the complex. In experiments this is done by substituting parts of the complexes[9,10,16,17,20] or by changing the polarity of the solvent.[16] Also the geometry and size of the bridge block can be varied, and in this way the length of the subsystem through which the electron has to be transferred[9,11,20−23] can be changed.

Superexchange occurs because of coherent mixing of the three or more states of the system.[14,15,24,25] The ET rate in this channel depends algebraically on the differences between the energy levels[9,10] and decreases exponentially with increasing bridge length.[14,23,25] When incoherent effects such as dephasing dominate, the transfer is mainly sequential,[12,23] that is, the levels are occupied mainly in sequential order.[5,12,13,16] The dependence on the differences between the energy levels is exponential.[9,10] An increase of the bridge length induces only a small reduction in the ET rate.[5,21,23,25,26] This is why sequential transfer is the desired process in molecular wires.[23,27]

In the superexchange case the dynamics is mainly Hamiltonian and can be described on the basis of the Schrödinger equation. The physically important results can be obtained by perturbation theory[14,28] and, most successfully, by the semiclassical Marcus theory.[6] The complete system dynamics can be directly extracted by numerical diagonalization of the Hamiltonian.[23,29] In case of sequential transfer the influence of an environment has to be taken into account. There are quite a few different ways of how to include an environment modeled by a heat bath. The simplest phenomenological descriptions are based on the Einstein coefficients or on the imaginary terms in the Hamiltonian,[30,31] as well as on the Fokker−Planck or Langevin equations.[30,31] The most accurate but also numerically most expensive way is the path integral method.[30] This has been applied to bridge-mediated ET, especially in the case of bacterial photosynthesis.[32] Bridge-mediated ET has also been investigated using Redfield theory,[13,33] by propagating a density matrix (DM) in Liouville space,[12] and other methods.[25,29,34−36]

The purpose of the present investigation is to present a simple, analytically solvable model based on the DM formalism[37,38] and apply it to a porphyrin−quinone complex, which is taken as a model system for the bacterial photosynthetic reaction center. The master equation that governs the DM evolution as well as the appropriate relaxation coefficients can be derived from such basic information as system−environment coupling strength and spectral density of the environment.[37−45] In the present model, relaxation is introduced in a way similar to Redfield theory but in site representation, not in eigenstate representation. A discussion of advantages and disadvantages of these representations has been given elsewhere.[46] The equations for the DM are the same as in the generalized stochastic Liouville equation (GSLE) model[47,48] for exciton transfer, which is an extension

10.1021/jp994338v CCC: $19.00
Published on Web 05/20/2000

of the Haken−Strobl−Reineker (HSR) model[49,50] to a model with a quantum bath. Here we give an analytic solution to these equations. The present equations for the DM obtained are also similar to those of ref 11, where relaxation is introduced in a phenomenological fashion but only a steady-state solution is found, in contrast to the model introduced here. In addition, the present model is applied to a concrete system. A comparison of the ET time with the bath correlation time allows us to regard three time intervals of system dynamics: the interval of memory effects, the dynamical interval, and the kinetic, long-time interval.[49] In the framework of DM theory one can describe the ET dynamics in all three time intervals. However, often it is enough to find the solution in the kinetic interval for the explanation of experiments within the time resolution of most experimental setups, as has been done in refs 11 and 51. The master equation is analytically solvable only for simple models, for example, refs 31 and 52. Most investigations are based on the numerical solution of this equation.[12,26,40,43] Here we perform numerical as well as approximate analytical calculations for a simple model. Because the solution can be easily obtained, the influence of all parameters on the ET can be examined.

The paper is organized as follows. In the next section the model of a supermolecule that we use to describe ET processes is introduced. The properties of an isolated supermolecule are modeled in subsection II A, as well as the static influence of the environment. The dynamical influence of bath fluctuations is discussed and modeled by a heat bath of harmonic oscillators in section II B. The reduced DM equation of motion (RDMEM) describing the excited-state dynamics is presented in subsection II C. In subsection II D the system parameter dependence on the solvent dielectric constant is discussed for different models of solute−solvent interaction. In subsection II E the system parameters are determined. The methods and results of the numerical and analytical solutions of the RDMEM are presented in section III. Dependencies of the ET rate and final acceptor population on the system parameters are given for the numerical and analytical solutions in subsection IV A. The analysis of the physical processes in the system is also performed there. In subsection IV B we discuss the dependence of the ET rate on the solvent dielectric constant for different models of solute−solvent interaction and compare the calculated ET rates with the experimentally measured ones. The advantages and disadvantages of the presented method in comparison with the GSLE model[47,48] and the method of Davis et al.[11] are analyzed in subsection IV C. In the conclusions the achievements and possible extensions of this work are discussed.

II. Model

A. System Part of the Hamiltonian. The photoinduced ET in supermolecules consisting of three sequentially connected molecular blocks indicated by index M, that is, donor ($M = 1$), bridge ($M = 2$), and acceptor ($M = 3$), is analyzed. The donor is not able to transfer its charge directly to the acceptor because of their spatial separation. Donor and acceptor can exchange their charges only through the bridge. In the present investigation the supermolecule consists of free-base tetraphenylporphyrin (H_2P) as donor, zinc-substituted tetraphenylporphyrin (ZnP) as bridge, and *p*-benzoquinone (Q) as acceptor.[16] In each of those molecular blocks we consider only two molecular orbitals ($m = 0,1$), the highest occupied molecular orbital (HOMO, $m = 0$) and the lowest unoccupied molecular orbital (LUMO, $m = 1$).[53] Each of these orbitals can be occupied by an electron or not, denoted by $|1\rangle$ or $|0\rangle$, respectively. This model allows us to describe four states of each molecular block, the neutral ground state $|1\rangle_{\mathrm{HOMO}}|0\rangle_{\mathrm{LUMO}}$, the neutral excited state $|0\rangle_{\mathrm{HOMO}}|1\rangle_{\mathrm{LUMO}}$, the positively charged ionic state $|0\rangle_{\mathrm{HOMO}}|0\rangle_{\mathrm{LUMO}}$, and the negatively charged ionic state $|1\rangle_{\mathrm{HOMO}}|1\rangle_{\mathrm{LUMO}}$. $c^{+}_{Mm} = |1\rangle_{Mm}\langle 0|_{Mm}$, $c_{Mm} = |0\rangle_{Mm}\langle 1|_{Mm}$, and $\hat{n}_{Mm} = c^{+}_{Mm}c_{Mm}$ describe the creation, annihilation, and number of electrons in orbital Mm, respectively, whereas $\hat{n}_M = \sum_m \hat{n}_{Mm}$ gives the number of electrons in a molecular block. The number of particles in the whole supermolecule is conserved, $\sum_M \hat{n}_M = \text{const}$.

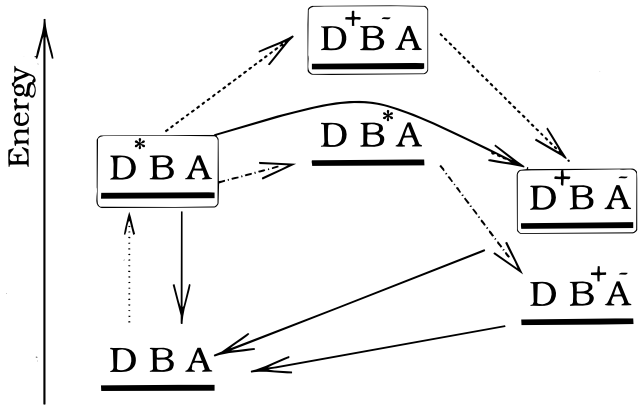

Figure 1. Schematic presentation of energy levels in the $H_2P-ZnP-Q$ complex. The three states in the boxes play the main role in ET, which can happen either sequentially or by a superexchange mechanism. Dashed lines refer to sequential transfer, curved solid line to superexchange, dot−dashed to energy transfer followed by ET, dotted line optical excitation, and straight solid lines either fluorescence or irradiative recombinations.

Each of the electronic states has its own vibrational substructure. As a rule for the porphyrin-containing systems the time of vibrational relaxation is 2 orders of magnitude faster than the characteristic ET time.[16] Because of this we assume that only the ground vibrational states play a role and we do not include the vibrational substructure. A comparison of the models with and without vibrational substructure has been given elsewhere.[54]

Below we consider the evolution of single charge-transfer exciton states in the system. For the full description of the system one also should include photon modes to describe for example the fluorescence from the LUMO to the HOMO in each molecular block transferring an excitation to the electromagnetic field. But the rates of fluorescence and recombination are small in comparison to other processes for porphyrin-type systems.[16,55] When fluorescence does not have to be taken into account, all states except $|\mathrm{D^*BA}\rangle$ (excited electron at site $M = 1$), $|\mathrm{D^+B^-A}\rangle$ (excited electron at site $M = 2$), and $|\mathrm{D^+BA^-}\rangle$ (excited electron at site $M = 3$) remain essentially unoccupied, whereas those three take part in the intermolecular transport process (see Figure 1). In this case the number of states coincides with the number of sites in the system and we label the states $|\mathrm{D^*BA}\rangle$, $|\mathrm{D^+B^-A}\rangle$, $|\mathrm{D^+BA^-}\rangle$ with the indices $\mu = 1, 2, 3$, respectively. Thus that the index of state μ reflects the localization of the excited electron at site M. This coincidence is used below for labeling the number operator $\hat{n}$ for the electrons, the interblock hopping term $\hat{V}$, etc.

For the description of the ET and other dynamical processes in the system placed in a dissipative environment we introduce the Hamiltonian

$$\hat{H} = \hat{H}_{\mathrm{S}} + \hat{H}_{\mathrm{B}} + \hat{H}_{\mathrm{SB}} \tag{1}$$

where $\hat{H}_{\mathrm{S}}$ describes the supermolecule, $\hat{H}_{\mathrm{B}}$ the dissipative bath, and $\hat{H}_{\mathrm{SB}}$ their interaction. We are interested in the kinetic limit of the excited-state dynamics here. For this limit we assume

that the relaxation of the solvent takes only a very short time compared to the system times of interest.

The effect of the solvent is twofold. On one hand the system dynamics is perturbed by the solvent-state fluctuations, independent of the system states. $\hat{H}_{SB}$ shall only reflect the dynamical influence of the fluctuations leading to dissipative processes, as discussed in the next subsection. On the other hand the system states are shifted in energy,[56]

$$\hat{H}_S = \hat{H}_0 + \hat{H}_{es} + \hat{V} \tag{2}$$

because of the static influence of the solvent, which is determined by the relaxed value of the solvent polarization and in general also includes the nonelectrostatic contributions such as van der Waals attraction, short-range repulsion, and hydrogen bonding.[57,58] In eq 2 the energy of free and noninteracting blocks $\hat{H}_0 = \sum_{Mm} E_{Mm} \hat{n}_{Mm}$, is given by the energies E_{Mm} of orbitals Mm in the independent electron approximation.[4,59] The E_{Mm} are chosen to reproduce the ground-state−excited-state transitions, for example, D → D*, which change only a little for different solvents[16] and are assumed to be constants here. To determine E_{Mm} one starts from fully ionized double bonds in each molecular block,[59] calculates the one-particle states, and fills these orbitals with two electrons each, starting from the lowest energy. By exciting, removing, and adding the last electron to the model system one obtains the energy of the excited, oxidized, reduced molecular block in the independent particle approximation.

The interblock hopping term

$$\hat{V} = \sum_{\mu\nu} v_{\mu\nu} (\hat{V}^+_{\mu\nu} + \hat{V}_{\mu\nu}) [(\hat{n}_\mu - 1)^2 + (\hat{n}_\nu - 1)^2]$$

in eq 2 includes the operators of electron hopping $\hat{V}_{\mu\nu} = c^+_{N1} c_{M1}$ from the excited state (LUMO) at site M to the excited state (LUMO) at site N and the coherent couplings $v_{\mu\nu}$. As aforementioned, the index μ can also be used to denote the location of the excited electron. Because of the analogy of the site index M and state index μ, the operator $\hat{n}_\mu$ represents the number of electrons at site M. We assume $v_{13} = 0$ because there is no direct connection between donor and acceptor. The scaling of $v_{\mu\nu}$ for different solvents is discussed in subsection II D.

The electrostatic interaction $\hat{H}_{es}$ enters into the system part of the Hamiltonian eq 2. It scales like the energies in a system of charges surrounded by a medium with static dielectric constant ϵ_s according to the classical reaction field theory.[60] Here we consider two scaling models. In the first model each molecular block is in an individual cavity in the dielectric. For this case the electrostatic energy reads

$$\hat{H}_{es} = S^H(\epsilon_s)\,(\hat{H}_{el} + \hat{H}_{ion}) \tag{3}$$

$$\hat{H}_{el} = \sum_\mu |\hat{n}_\mu - 1| e^2 (4\pi\epsilon_0 r_\mu)^{-1}$$

takes the electron interaction into account while bringing an additional charge onto the block μ and thus describes the energy to create an isolated ion. This term depends on the characteristic radius r_μ of the molecular block. The interaction between the ions

$$\hat{H}_{ion} = \sum_\mu \sum_\nu (\hat{n}_\mu - 1)(\hat{n}_\nu - 1) e^2 (4\pi\epsilon_0 r_{\mu\nu})^{-1}$$

depends on the distance between the molecular blocks $r_{\mu\nu}$. Both distances r_μ and $r_{\mu\nu}$ are also used in Marcus theory.[6] The term $H_{el} + H_{ion}$ reflects the interaction of charges inside the supermolecule, which is weakened by the reaction field according to the Born formula[61]

$$S^H = 1 + \frac{1 - \epsilon_s}{2\epsilon_s} \tag{4}$$

In the second model, considering the supermolecule as one object placed in a single cavity of constant radius, one has to use the Onsager term.[61] This term is state-selective; it gives a contribution only for the states with nonzero dipole moment, that is, charge separation. Defining the static dipole moment operator as

$$\hat{p} = \sum_{\mu\nu} (\hat{n}_\mu - 1)(\hat{n}_\nu - 1) \vec{r}_{\mu\nu} e$$

we obtain $\hat{H}_{es} = S^H \hat{p}^2 / r_{13}$, with Onsager scaling

$$S^H = \frac{1 - \epsilon_s}{2\epsilon_s + 1} \tag{5}$$

B. Microscopic Motivation of System−Bath Interaction and Thermal Bath. One can express the dynamic part of the system−bath interaction as

$$\hat{H}_{SB} = -\int d^3\vec{r} \sum_{\mu\nu} \hat{D}_{\mu\nu}(\vec{r}) \Delta\hat{P}(\vec{r}) \tag{6}$$

Here $\hat{D}_{\mu\nu}(\vec{r})$ denotes the field of the electrostatic displacement at point $\vec{r}$ induced by the system transition dipole moment $\hat{p}_{\mu\nu} = \vec{p}_{\mu\nu}(\hat{V}^+_{\mu\nu} + \hat{V}_{\mu\nu})$.[31] The field of the environmental polarization is denoted as $\hat{P}(\vec{r}) = \sum_n \delta(\vec{r} - \vec{r}_n)\hat{d}_n$, where $\hat{d}_n$ is the nth dipole of the environment and $\vec{r}_n$ its position. Only fluctuations of the environment polarization $\Delta\hat{P}(\vec{r})$ influence the system dynamics. Averaged over the angular dependence the interaction reads[56]

$$\hat{H}_{SB} = -\sum_{\mu\nu n} \frac{1}{4\pi\epsilon_0} \left(\frac{2}{3}\right)^{1/2} \frac{|\hat{p}_{\mu\nu}| \Delta|\hat{d}_n|}{|\vec{r}_n|^3} \tag{7}$$

The dynamical influence of the solvent is described with a thermal bath model. The deviation $\Delta|\hat{d}_n|$ of d_n from its mean value is determined by temperature-induced fluctuations. For unpolar solvents described by a set of harmonic oscillators the diagonalization of their interaction yields a bath of harmonic oscillators with different frequencies ω_λ and effective masses m_λ. In the case of a polar solvent the dipoles are interacting rotators as, for example, used to describe magnetic phenomena.[62,63] The elementary excitation of each frequency can again be characterized by an appropriate harmonic oscillator. So we use generalized coordinates of solvent harmonic oscillator modes $\hat{Q}_\lambda = \sqrt{\hbar (2 m_\lambda \omega_\lambda)^{-1}} (\hat{a}_\lambda + \hat{a}^+_\lambda)$ for polar as well as unpolar solvents. The occupation of the ith state of the λth oscillator is defined by the equilibrium DM $\rho_{\lambda,ij} = \exp[-\hbar\omega_\lambda i/(k_B T)]\delta_{ij}$.

All mutual orientations and distances of solvent molecules have equal probability. An average over all spatial configurations is performed. The interaction Hamiltonian (eq 7) is written in a form that is bilinear in system and bath operators:

$$\hat{H}_{SB} = [\sum_{\mu\nu} p_{\mu\nu} (\hat{V}_{\mu\nu} + \hat{V}^+_{\mu\nu})][\sum_\lambda K_\lambda (\hat{a}^+_\lambda + \hat{a}_\lambda)] S_{SB} \tag{8}$$

$p_{\mu\nu} K_\lambda$ denotes the interaction intensity between the bath mode

a_λ of frequency ω_λ and the quantum transition between the LUMOs of molecules μ and ν with frequency $\omega_{\mu\nu} = (E_\mu - E_\nu)/\hbar$. The scaling function S_{SB} reflects the properties of the solvent. Explicit expressions for the solvent influence are still under discussion in the literature.[57,58]

C. Reduced Density Matrix Approach. The interaction of the system with the bath of harmonic oscillators describes the irradiative energy transfer from the system to the solvent as modeled by eq 8. Radiative processes are neglected here because of the much longer time scales. For the description of the dynamics we use the reduced DM, which can be obtained from the full DM ρ by tracing over the environmental degrees of freedom $\sigma = Tr_B\rho$[38] with the evolution operator technique,[18,64] restricting ourselves to the second-order cumulant expansion.[65]

At this point we recall that the electrostatic interaction $\hat{H}_{es}$ is included in the energies of the system states. The electronic coupling $\hat{V}$ between the states is not included into the projection procedure. This approximation has been performed for the sake of simplicity. For the transitions between Schrödinger and Heisenberg pictures as used in the evaluation of the RDMEM, one needs the explicit form of the system Hamiltonian, which is much simpler in the limit $\hat{V} \rightarrow 0$. In principle one can eliminate $\hat{V}$ by diagonalizing $\hat{H}_S$. This method is referred to as the adiabatic approach or eigenstate representation.[46] In general to apply it, the eigenvalues have to be calculated numerically. Instead, we use the site representation (diabatic approach), that is, while evaluating the RDMEM, $\hat{V}$ is set to 0. The condition of applicability of the diabatic approach, $v^0_{\mu\nu} \ll \hbar\omega_{\mu\nu}$, is discussed in subsection IV C.

After tracing out the bath, we apply the Markov approximation, that is, we restrict ourselves to the limit of long times. Furthermore, the discrete set of bath modes is replaced with a continuous one. To do so one has to introduce the spectral density of bath modes $J(\omega) = \pi\sum_\lambda K^2_\lambda(\omega - \omega_\lambda)$. Finally one obtains the following master equation

$$\dot{\sigma}_{\kappa\lambda} = -\frac{i}{\hbar}([\hat{H}_S, \sigma])_{\kappa\lambda} + 2\delta_{\kappa\lambda}\sum_\mu\{\Gamma_{\mu\kappa}[n(\omega_{\mu\kappa}) + 1] + \Gamma_{\kappa\mu}n(\omega_{\kappa\mu})\}\sigma_{\mu\mu} - \sum_\mu\{\Gamma_{\mu\kappa}[n(\omega_{\mu\kappa}) + 1] + \Gamma_{\kappa\mu}n(\omega_{\kappa\mu}) + \Gamma_{\mu\lambda}[n(\omega_{\mu\lambda}) + 1] + \Gamma_{\lambda\mu}n(\omega_{\lambda\mu})\}\sigma_{\kappa\lambda} + \{\Gamma_{\lambda\kappa}[2n(\omega_{\lambda\kappa}) + 1] + \Gamma_{\kappa\lambda}[2n(\omega_{\kappa\lambda}) + 1]\}\sigma_{\lambda\kappa} \quad (9)$$

where $n(\omega) = [\exp(\hbar\omega/k_BT) - 1]^{-1}$ denotes the Bose−Einstein distribution. The damping constant

$$\Gamma_{\mu\nu} = S^2_{SB}\hbar^{-2}J(\omega_{\mu\nu})p^2_{\mu\nu} \quad (10)$$

reflects the coupling of the transition $|\mu\rangle \rightarrow |\mu\rangle$ to a bath mode of the same frequency. It depends on the density of bath modes J at the transition frequency $\omega_{\mu\nu}$ and on the transition dipole moments $p_{\mu\nu}$. A RDMEM of similar structure was used for the description of exciton transfer in the HSR model[49,50] and the GSLE model.[47,48] The HSR method originating from the stochastic bath model is valid only in the high-temperature limit.[48] The GSLE method[47,48] is a model with a quantum bath and system−bath coupling of the form $\hat{H}_{SB} \sim \hat{V}^+\hat{V}(\hat{a}^+_\lambda + \hat{a}_\lambda)$, which modulates the system transition frequencies. In refs 47 and 48 the equations for exciton motion are derived using the projection operator technique. Taking the different system−bath coupling we have derived the RDMEM, which coincides with the GSLE.[47,48] Both GSLE and our RDMEM are able to describe correctly finite temperatures. Below, we neglect the last term of eq 9 corresponding to the $\bar{\gamma}$ term in the HSR and GSLE models because the rotating wave approximation is applied.

For the sake of convenience of the analytical and numerical calculations we replace $\Gamma_{\mu\nu}$ and the population of the corresponding bath mode $n(\omega_{\mu\nu})$ with the dissipative transitions $d_{\mu\nu} = \Gamma_{\mu\nu}|n(\omega_{\mu\nu})|$ and the corresponding dephasings $\gamma_{\mu\nu} = \sum_\kappa(d_{\mu\kappa} + d_{\kappa\nu})/2$. With this, one can express the RDMEM (eq 9) in the form

$$\dot{\sigma}_{\mu\mu} = -i/\hbar\sum_\nu(v_{\mu\nu}\sigma_{\nu\mu} - \sigma_{\mu\nu}v_{\nu\mu}) - \sum_\nu d_{\mu\nu}\sigma_{\mu\mu} + \sum_\nu d_{\nu\mu}\sigma_{\nu\nu} \quad (11)$$

$$\dot{\sigma}_{\mu\nu} = (-i\omega_{\mu\nu} - \gamma_{\mu\nu})\sigma_{\mu\nu} - i/\hbar v_{\mu\nu}(\sigma_{\nu\nu} - \sigma_{\mu\mu}) \quad (12)$$

The parameters controlling the transitions between the selected states are discussed in subsection II E.

D. Scaling of Damping Constants. The relaxation coefficients of eq 10 include the second power of the scaling function S_{SB} because second-order perturbation theory in the system−bath coupling is used. The physical meaning of H_{SB} is similar to the interaction of the system dipole with the surrounding media. That is why it is reasonable to use the Onsager expression (eq 5) for S_{SB}. In the work of Mataga et al.[66] the interaction energy between the system dipole and the media scales in leading order is

$$S_{SB} = -\left[\frac{2(\epsilon_s - 1)}{2\epsilon_s + 1} - \frac{2(\epsilon_\infty - 1)}{2\epsilon_\infty + 1}\right] \quad (13)$$

where ϵ_∞ denotes the optical dielectric constant. From a recent paper of Georgievskii et al.[57] we extract

$$\Gamma \sim \frac{1}{\epsilon_s} - \frac{1}{\epsilon_\infty}$$

for the multiple cavities model assuming $\epsilon_\omega = \epsilon_\infty$. In terms of a scaling function it can be expressed as

$$S_{SB} = (1/\epsilon_s - 1/\epsilon)^{1/2} \quad (14)$$

As we have already argued in ref 54, the coherent coupling $v_{\mu\nu}$ between two electronic states scales with ϵ_s and ϵ_∞ too, because a coherent transition in the system is accompanied by a transition of the environment state, which is larger for solvents with larger polarity. As discussed above, we neglect the vibrational substructure of each electronic state because the vibrational relaxation is about 2 orders of magnitude faster than the characteristic ET time. But in contrast to the model with vibrational substructure, the present model does not involve any reaction coordinate. To reproduce the results of the more elaborate model with vibrational substructure, one has to scale the electronic couplings $v_{\mu\nu}$ with the Franck−Condon overlap elements $F_{FC}(\mu,0,\nu,0)$ between the vibrational ground states of each pair of electronic surfaces

$$v_{\mu\nu} = v^0_{\mu\nu}F_{FC}(\mu, 0, \nu, 0) \quad (15)$$

where $v^0_{\mu\nu}$ is the coupling of electronic states of the isolated molecule. For the calculation of the Franck−Condon factors one has to introduce the leading (mean) environment oscillator frequency ω_{vib}. Here $\omega_{vib} = 1500\ cm^{-1}$ is used, which is similar to the frequency of the C−C stretching mode. With this scaling one implicitly introduces a reaction coordinate into the model.

TABLE 1: Energy of Charged Bridge State in Different Solvents and Corresponding ET Rates

solution	CH_2Cl_2	MTHF	CYCLO
ϵ_s, ref 67	9.08	6.24	2.02
$E_{D^+B^-A}$, eV	3.12	3.18	3.59
k_{ET}, 10^7 s^{-1}, numerical[a]	33	36	0.46
k_{ET}, 10^7 s^{-1}, analytical[a]	33	36	0.46
k_{ET}, 10^7 s^{-1}, experimental[16]	23 ± 5	36 ± 5	$0 + 3$

[a] For calculations, born scaling (eq 4) of energy and Marcus scaling (eq 14) of dissipation are used.

E. Model Parameters. The dynamics of the system is controlled by the following parameters: energies of system states E_μ, coherent couplings $v_{\mu\nu}$, and damping constants $\Gamma_{\mu\nu}$.

On the basis of the spectral data[62] and taking $E_{DBA} = 0$ as reference energy we determine $E_{D*BA} = 1.82$ eV (in CH_2Cl_2). We take the energy of the state with ET to Q from ref 16: $E_{D^+BA^-} = 1.42$ eV.[68] Further, Rempel et al.[16] estimate the coupling of initially excited and charged bridge states $\langle D^*BA|H|D^+B^-A\rangle = v_{12}^0 = 65$ meV $= 9.8 \times 10^{13}$ s^{-1} and the coupling of the two states with charge separation $\langle D^+B^-A|H|D^+BA^-\rangle = v_{23}^0 = 2.2$ meV $= 3.3 \times 10^{12}$ s^{-1}. The values of the couplings are essentially lower than the energy differences between the relevant system states

$$\hbar\omega_{\mu\nu} \gg v_{\mu\nu}^0 \tag{16}$$

This is the reason to remain in site representation instead of eigenstate representation.[46] The damping constants are found with help of the analytical solution derived at the end of the next section to be $\Gamma_{21} = \Gamma_{23} = 2.25 \times 10^{12}$ s^{-1}. The typical radius of the porphyrin ring is about $r_\mu = 5 \pm 1$ Å,[17] while the distance $r_{\mu\nu}$ between the blocks of $H_2P-ZnP-Q$ reaches $r_{12} = 12.5 \pm 1$ Å,[16,17] $r_{23} = 7 \pm 1$ Å, $r_{13} = 14 \pm 1$ Å. The main parameter that controls ET in a triad is the energy of the state $E_{D^+B^-A}$. This state has a big dipole moment because of its charge separation and is therefore strongly influenced by the solvent. Because of the special importance of this value we calculate it for the different solvents as a matrix element of the system Hamiltonian (eq 2). The calculated values of the energies of the D^+B^-A state for some solutions are shown in Table 1.

III. Results

The time evolution of the ET in the supermolecule is described by solving eqs 11 and 12 numerically and analytically. As an initial condition, the donor population is set to one, which can be reached by a π pulse of appropriate frequency.

For the numerical simulation we express the system of eqs 11 and 12 in the form $\dot{\bar{\sigma}} = A\bar{\sigma}$, where $\bar{\sigma}$ is a vector of dimension 3^2 for the model with 3 system states and the superoperator A is a matrix of dimension $3^2 \times 3^2$. We find an exponential growth of the acceptor population

$$P_3(t) = P_3(\infty)[1 - \exp(-k_{ET}t)] \tag{17}$$

where for the solvent 2-methyltetrahydrofuran (MTHF) $k_{ET} \simeq 3.59 \times 10^8$ s^{-1} and $P_3(\infty) \simeq 0.9994$. The population P_2, which corresponds to charge localization on the bridge, does not exceed 0.005. This means that in this case the superexchange mechanism dominates over the sequential transfer mechanism. Besides, it ensures the validity of characterizing the system dynamics with $P_3(\infty)$ and

$$k_{ET} = P_3(\infty)\{\int_0^\infty [P_3(\infty) - P_3(t)]dt\}^{-1} \tag{18}$$

The alternative analytical approach is performed in the kinetic limit

$$t \gg 1/\min(\gamma_{\mu\nu}) \tag{19}$$

In Laplace space the inequality (eq 19) reads $s \ll \min(\gamma_{\mu\nu})$, where s denotes the Laplace variable. It is equivalent to replacing the factor $1/(i\omega_{\mu\nu} + \gamma_{\mu\nu} + s)$ in the Laplace transform of eqs 11 and 12 with $1/(i\omega_{\mu\nu} + \gamma_{\mu\nu})$. This trick allows us to substitute the expressions eq 12 for nondiagonal elements of the DM into eq 11. After this elimination we describe the coherent transitions to which the nondiagonal elements contribute by redefinition of the diagonal RDMEM (eq 11)

$$\dot{\sigma}_{\mu\mu} = -\sum_\nu g_{\mu\nu}\sigma_{\mu\mu} + \sum_\nu g_{\nu\mu}\sigma_{\nu\nu} \tag{20}$$

The transition coefficients $g_{\mu\nu}$ contain dissipative and coherent contributions

$$g_{\mu\nu} = d_{\mu\nu} + v_{\mu\nu}v_{\nu\mu}\gamma_{\mu\nu}[\hbar^2(\omega_{\mu\nu}{}^2 + \gamma_{\mu\nu}{}^2)]^{-1} \tag{21}$$

Now it is assumed that the bridge is not populated. This allows us to find the acceptor population in the form of eq 17, where

$$k_{ET} = g_{32} + g_{23}(g_{12} - g_{32})(g_{21} + g_{23})^{-1} \tag{22}$$

$$P_3(\infty) = g_{12}g_{23}[(g_{21} + g_{23})k_{ET}]^{-1} \tag{23}$$

The value of $\Gamma_{\mu\nu} = S_{SB}^2\hbar^{-2}J(\omega_{\mu\nu})p_{\mu\nu}^2$ can be found comparing the experimentally determined ET rate and eq 22. To calculate $J(\omega_{\mu\nu})$ would require a microscopic model. To avoid a microscopic consideration we simply take the same $\Gamma_{\mu\nu}$ for all transitions between excited states. The value of ET for $H_2P-ZnP-Q$ in MTHF is found by Rempel et al.[16] to be $k_{ET} = 3.6 \pm 0.5 \times 10^8$ s^{-1}. In the systems considered here the coefficients g_{21},g_{23} are of order of magnitude 10^{12} s^{-1}, g_{12} of order 10^8 s^{-1}, and g_{32} of order 10^6 s^{-1}. If the bridge state has a rather high energy, one can neglect thermally activated processes ($d_{12} = d_{32} = 0$). For the deactivation processes the dissipative terms are stronger than the coherent ones ($g_{21} = d_{21}$, $g_{23} = d_{23}$). The coupling v_{23} is negligibly small with respect to v_{12}. In this case eq 22 reads

$$k_{ET} = v_{12}^2\Gamma_{21}\Gamma_{23}(\hbar^2\omega_{21}^2 + \Gamma_{21}^2)^{-1}(\Gamma_{21} + \Gamma_{23})^{-1} \tag{24}$$

With the relation $\Gamma_{21} = \Gamma_{23}$ and the experimental k_{ET}, one obtains $\Gamma_{21} = \Gamma_{23} \simeq 2.25 \times 10^{12}$ s^{-1}. The fit of the numerical solution of eqs 11 and 12 to the experimental k_{ET} in MTHF gives the same value. So the damping constants are fixed for a specific solvent, and for other solvents they are calculated with the scaling functions. With this method the ET was found to be dominated by the superexchange mechanism with rates 4.6×10^6 s^{-1} for cyclohexane (CYCLO) and 3.3×10^8 s^{-1} for CH_2Cl_2.

IV. Discussion

A. Sequential Versus Superexchange. To discuss how the transfer mechanism depends on the change of parameters we calculate the system dynamics varying one parameter at a time. The dependencies of k_{ET} and $P_3(\infty)$ on v_{12}, v_{23} and Γ_{21}, Γ_{23} are shown in Figures 2 and 3. The change of each parameter influences the transfer in a different way. In particular, k_{ET} depends quadratically on v_{12} from 10^{15} s^{-1} to 10^{12} s^{-1} in Figure

2. Below it saturates at the lower bound $k_{ET} \propto 3 \times 10^5\ s^{-1}$. This corresponds to a crossover of the ET mechanism from superexchange to sequential transfer. But, because of the big energy difference between donor and bridge states, the sequential transfer efficiency is extremely low. This is displayed by $P_3(\infty) \simeq 0$. In the region $v_{12} \approx v_{13}$ both mechanisms contribute to k_{ET}. The decrease of $P_3(\infty)$ in this region corresponds to coherent back transfer. The ET rate depends on v_{23} in a similar way. At rather high values of v_{12}, $v_{23} \simeq 10^{15}\ s^{-1}$, the relation (eq 16) is no longer valid. For this regime one has to use eigenstate instead of site representation because the wave functions are no longer localized.[46]

The variation Γ_{21}, Γ_{23} near the experimental values shows similar behavior of $k_{ET}(\Gamma_{21})$ and $k_{ET}(\Gamma_{23})$ (see Figure 3). Here we independently vary Γ_{21} and Γ_{23}. Both $k_{ET}(\Gamma_{21})$ and $k_{ET}(\Gamma_{23})$ increase linearly until the saturation value $7 \times 10^8\ s^{-1}$ at $\Gamma > 10^{12}\ s^{-1}$ is reached. The numerical and analytical values agree qualitatively. In eq 18 infinite time is approximated by 10^{-5} s and so one cannot obtain ET rates lower than this limit.

The physical meaning of the ET rate dependence on Γ seems to be transparent. At small values of Γ a part of the population coherently oscillates back and forth between the states. The increase of the dephasing $\gamma_{\mu\nu}$ quenches the coherence and makes the transfer irreversible. So transfer becomes faster up to a maximal value. For the whole range of Γ, depopulations d_{12}, d_{23} and thermally activated transitions d_{12}, d_{32} always remain smaller than the coherent couplings; therefore they do not play an essential role.

Next, the similarity of the dependencies on Γ_{21} and Γ_{23} will be discussed on the basis of eq 22. In the limit $k_B T/\hbar\omega_{\mu\nu} \rightarrow 0$ thermally activated processes with $\omega_{\mu\nu} < 0$ vanish and so $|n(\omega_{\mu\nu})| = 0$, wherever depopulations with $\omega_{\mu\nu} > 0$ remain constant $|n(\omega_{\mu\nu}) = 1$. The condition $\omega_{\mu\nu} \gg \gamma_{\mu\nu}$ allows us to neglect $\gamma_{\mu\nu}^2$ in comparison with $\omega_{\mu\nu}^2$. With these simplifications eq 22 becomes

$$k_{ET} \simeq \Gamma_{21}\Gamma_{23}(\Gamma_{21} + \Gamma_{23})^{-1}(v_{12}^2/\omega_{21}^2 + v_{23}^2/v_{23}^2) \quad (25)$$

that is, symmetric with respect to Γ_{21} and Γ_{23}.

To the largest extent the mechanism of transfer depends on the bridge energy $E_{D^+B^-A}$ as presented in Figure 4. In different regions one observes different types of dynamics. For large bridge energies $E_{21} = E_{D^+B^-A} - E_{D^*BA} \gg 0$ the numerical and analytical solutions do not differ from each other. The transfer occurs with the superexchange mechanism. The ET rate reaches a maximal value of $10^{11}\ s^{-1}$ for low bridge energies.

While the bridge energy approaches the donor energy, the sequential transfer starts to contribute to the ET process. The traditional scheme of sequential transfer is obtained when donor, bridge, and acceptor levels are arranged in a cascade. In this region the analytical solution need not coincide with the numerical solution because the used approximations are no longer valid. For equal bridge and acceptor energies k_{ET} displays a small resonance peak in Figure 4a. When the bridge energy is lower than the acceptor energy the population gets trapped at the bridge. The finite value of k_{ET} for $E_{21} < E_{31}$ does not mean ET because $P_3(\infty) \rightarrow 0$. For the dynamic time interval $t < \gamma_{\mu\nu}^{-1}$ a part of the population tunnels force and back to the acceptor with k_{ET}. The analytical solution (eq 22) gives a constant rate for the regime $E_{21} < E_{31}$, whereas the numerical solution of eqs 11 and 12 is instable. This is because coherent oscillations of the population cannot be described by eqs 17 and 18. In Figure 4 the regime $E_{21} < E_{31}$ occurs for small E_{21} while E_{31} is kept constant and for large E_{31} while E_{21} remains constant.

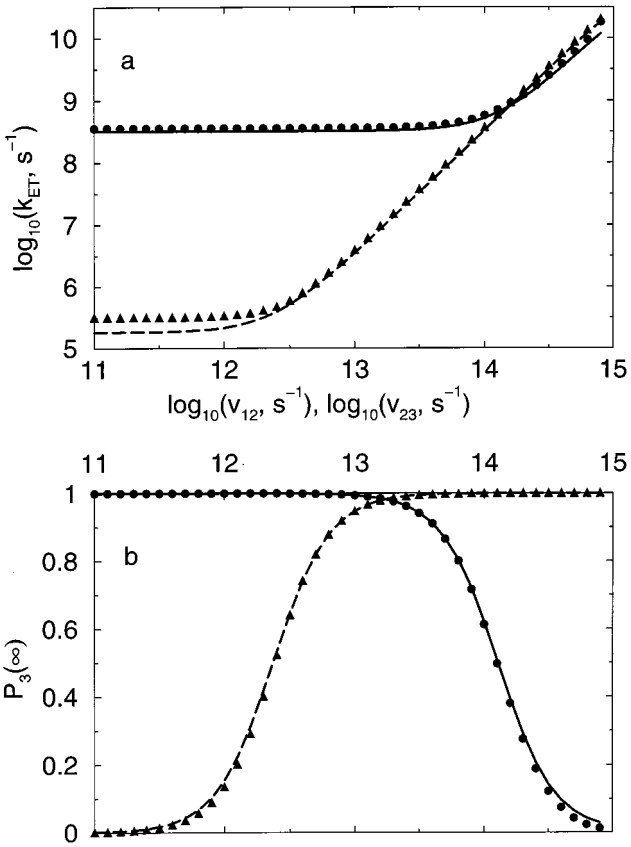

Figure 2. Dependence of ET rate (a) and final acceptor population (b) on coherent couplings v_{12} (triangles and dashed line, $v_{23} = v_{23}^0 = 2.2$ meV), v_{23} (dots and solid line $v_{12} = v_{12}^0 = 65$ meV). Symbols represent numerical solution of eqs 11 and 12, lines analytical solution (eqs 22 and 23).

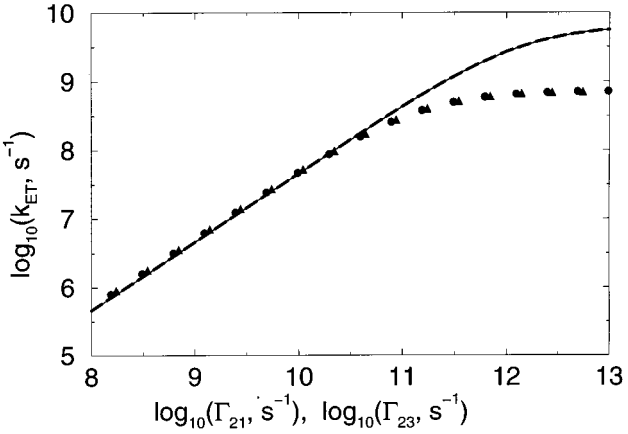

Figure 3. Dependence of ET rate on damping constants Γ_{21} (triangles and dashed line), Γ_{23} (dots and solid line). The other parameters correspond to $H_2P-ZnP-Q$ in MTHF. Symbols represent numerical and lines analytical solution.

The energy dependence of the final population has a transparent physical meaning for the whole range of energy. A large bridge energy ensures the transition of the whole population to the acceptor. In the intermediate case, when the bridge has the same energy as the acceptor, the final population is equally distributed on these two states $P_3(\infty) = 0.5$. Lowering the bridge even more, the whole population remains on the bridge as the lowest state of the system. The dependence of the ET rate on the acceptor energy $E_{31} = E_{D^+BA^-} - E_{D^*BA}$ in Figure 4 remains constant while the acceptor energy lies below the bridge energy. Increase of E_{31} up to $E_{21} = 1.36$ eV gives the

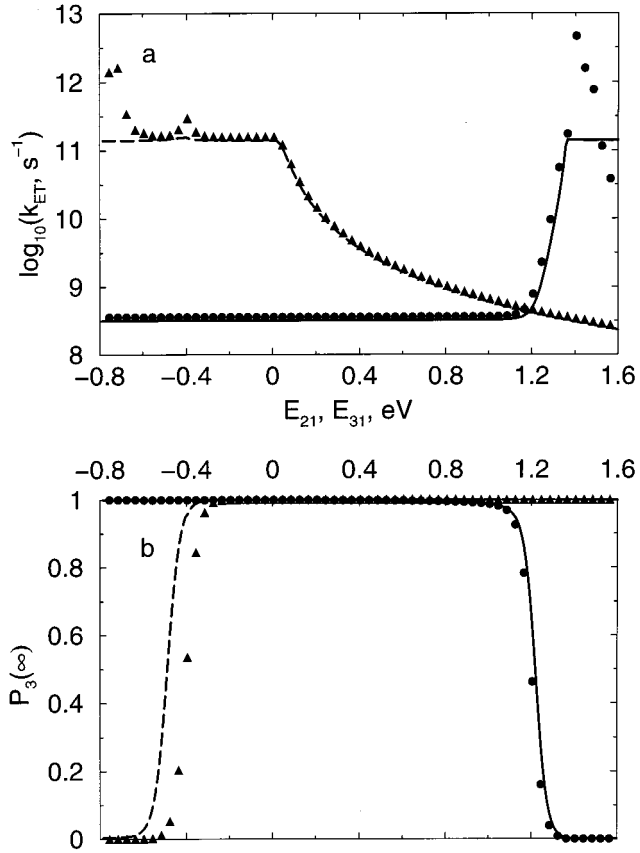

Figure 4. Dependence of ET rate (a) and final acceptor population (b) on energy of B $E_{21} = E_{D^+B^-A} - E_{D*BA}$ (triangles and dashed line, $E_{31} = -0.4$ eV) and A $E_{31} = E_{D^+BA^-} - E_{D*BA}$ (dots and solid line, $E_{21} = 1.36$ eV). Symbols represent numerical and lines analytical solution. $v_{12} = 65$ meV, $v_{23} = 2.2$ meV, $\Gamma_{21} = \Gamma_{23} = 2.25 \times 10^{12}$ s^{-1}.

maximal $k_{ET} \propto \Gamma_{21}$. When E_{31} increases further, the acceptor becomes the highest level in the system and therefore the population cannot remain on it.

B. Different Solvents. For the application of the results to various solvents and comparison with experiment, one should use the scaling for energy, coherent couplings, and damping constants as discussed above. The combinations of the energy scaling in subsection II A and damping constants scalings in subsection II D are represented in Figure 5. An increase in ϵ_s from 2 to 4 leads to an increase of the ET rate, no matter which scaling is used. Further increase of ϵ_s induces saturation for the Onsager−Mataga scaling and even a small decrease. Within the applied approximations an increase in the solvent polarizability and, consequently, of its dielectric constant lowers the bridge and acceptor energies and increases the system−bath interaction and, consequently, the relaxation coefficients. It induces a smooth rise of the ET rate for the Onsager−Mataga scaling. On the other hand, large ϵ_s leads to essentially different polarizational states of the environment for the supermolecule states with different dipole moment. This reduces the coherent couplings (see eq 15), leading for the Born−Marcus scaling to a small decrease of k_{ET} for large ϵ_s. The ET rate with this scaling comes closer to the experimental value $k_{ET}(\epsilon_s^{CH_2Cl_2})$. This gives a hint that the model of individual cavities for each molecular block is closer to reality than the model with a single cavity for the whole supermolecule.

Below we consider Born scaling eq 4 for the system energies and Marcus scaling eq 14 for the damping constant to compare the calculated ET rates with the measured ones. For the solvents

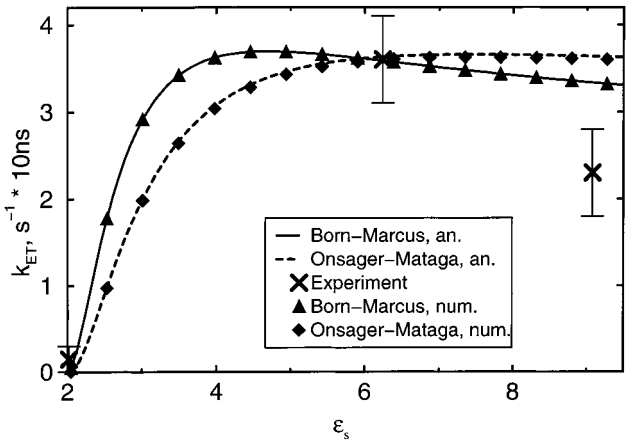

Figure 5. ET rate k_{ET} versus dielectric constant. The energies of the bridge and acceptor scale in accordance with Born expression (eq 4) (triangles and solid line), Onsager expression (eq 5) (diamonds and dashed line). Coherent couplings and damping constants scale in accordance with Mataga's expression (eq 13) (diamonds and dashed line), Georgievskii−Marcus expression (eq 14) (triangles and solid line). Symbols represent numerical and lines analytical solution. Solid crosses with error bars give experimental values.[16] Note that by using a different value of the damping parameter Γ, curves can be calculated that almost pass through all three experimental error bars.

CYCLO, MTHF, and CH_2Cl_2 one obtains the relative bridge energies $E_{21} = 1.77$, 1.36, and 1.30 eV, respectively.

The calculated ET rate coincides with the experimental value[16] for $H_2P-ZnP-Q$ in CYCLO (see Table 1). For CH_2Cl_2 the numerical ET rate is approximately 30% faster than the experimental value. It has to be noted that a value for the damping rates can be chosen such that the calculated curve almost passes through all three experimental error bars. On the other hand an error in the present calculation could be due to (a) absence of vibrational substructure of the electronic states in the present model; (b) incorrect dependence of system states energies on the solvent properties; (c) opening of additional transfer channels not mentioned in the scheme shown in Figure 1. Each of these possibilities needs some comments.

ad (a): The incorporation of the vibrational substructure will result in a complication of the model[13,54] giving a more complicated ET rate dependence on the energy of the electronic states and dielectric constant. It should yield the maximal ET rate for nonequal energies of electronic states, namely for the activationless case when the energy difference equals the reorganization energy. For a comparison of the models with and without vibrational substructure see ref 54.

ad (b): Effects such as the solvation shell[69] do need a molecular dynamics simulation. The total influence of the solvent is probably reflected in an energy shift between the spectroscopically observable states E_{D*BA} and E_{DB*A}.[16]

ad (c): A solvent with large ϵ_s can bring high-lying system states closer to the ones included in Figure 1; for example, because of its large dipole moment, $|D^-B^+A\rangle$ is strongly influenced by the solvent.

C. Comparison with Similar Theories. In the present calculations we have used the site representation (diabatic approach). There is some discussion in the literature about the precision of the results obtained within this approach.[46] Nevertheless, one uses the diabatic approach rather often[40,41] because it is less expensive numerically.[70] The applicability of the diabatic approach depends on the relations between coherent couplings and energy separations. The formalism derived in this paper has been applied to different regions of coupling values. One region corresponds to the variation of the coupling values

in Figure 2. This region is rather broad and includes those values that have been used for $H_2P-ZnP-Q$ with and without the scaling ansatz for $v_{\mu\nu}$. The relation $\hbar\omega_{\mu\nu} > v_{\mu\nu}$ holds for the whole region of coupling values presented in Figure 2. In most of the parameter range, $v_{\mu\nu}$ is even much smaller than $\hbar\omega_{\mu\nu}$. For the largest values of the coherent couplings presented in Figure 2 the site representation becomes problematic and the eigenstate representation is more appropriate. The error due to the application of the site representation for large values of the coupling has been estimated by Davis et al.[46] In their calculations the difference between dynamics in site and eigenstate representations remains rather small, even for large couplings. This difference disappears for high temperatures. Describing $H_2P-ZnP-Q$ without the scaling ansatz the values of the energies and couplings determined in subsection II E satisfy $\hbar\omega_{\mu\nu} \gg v_{\mu\nu}$. Thus one can use the site representation in this case. Applying the scaling function for the coherent coupling, one immediately finds that this function is always smaller than unity. Therefore in this case the coherent couplings are significantly smaller than the energy detuning.

As discussed above, the RDMEM are very similar to those of the GSLE model. This is an extension of the HSR theory in which a classical bath is used and for which analytical solutions are available.[48,49] We are not aware of any analytical solution of the GSLE model as presented here. Also, this model has not been applied to similar ET processes.

The numerical steady-state method used by Davis et al.[11] is an attractive one because of its simplicity, but unlike our method it is not able to give information about the time evolution of the system. We use a similar approach derived within a Redfield-like theory. But we consider dephasing and depopulation between each pair of levels. In contrast, Davis et al. incorporate relaxation phenomenologically only to selected levels; dephasing γ occurs between excited levels, whereas depopulation k takes place only for the sink from acceptor to the ground state. The advantage of the approach of Davis et al. is the possibility to investigate the ET rate dependence for the bridge consisting of more than one molecular block. This was not the goal of the present work, but it can be extended into this direction. We are interested in the ET in a concrete molecular complex with realistic parameter values and realistic possibilities to modify those parameters. Our results, as well as the results of Davis, show that ET can occur as coherent (with the superexchange mechanism) or dissipative processes (with the sequential transfer mechanism).

V. Conclusions

We have performed a study of the ET in the supermolecular complex $H_2P-ZnP-Q$ within the DM formalism. The determined analytical and numerical ET rates are in reasonable correspondence with the experimental data. The superexchange mechanism of ET dominates over the sequential transfer. We have investigated the stability of the model varying one parameter at a time. The qualitative character of the transfer is stable with respect to a local change of system parameter. The crossover between the two transfer mechanisms can be induced by lowering the bridge energy. The relation of the theory presented here to other theoretical approaches to ET has been discussed.

The calculations performed in the framework of the present formalism can be extended in the following directions: (a) Considerations beyond the kinetic limit. The vibrational substructure has to be included into the model as well as solvent dynamics and, probably, non-Markovian RDMEM. (b) Enlargement of the number of molecular blocks in the complex; (c) initial excitation of states with rather high energy should open additional transfer channels.

Acknowledgment. D.K. thanks U. Rempel and E. Zenkevich for stimulating discussions. Financial support of the DFG is gratefully acknowledged.

References and Notes

(1) Jortner, J., Bixon, M., Eds. *Adv. Chem. Phys.* **1999**, *106* and *107*.
(2) DeVault, D. *Quantum Mechanical Tunneling in Biological Systems;* Cambridge University Press: Cambridge, 1993.
(3) Balzani, V.; Scandola F. *Supramolecular Photochemistry;* Ellis Horwood: Chichester, 1991.
(4) Newton, M. *Chem. Rev.* **1991**, *91*, 767.
(5) Barbara, P. F.; Meyer, T. J.; Ratner, M. A. *J. Phys. Chem.* **1996**, *100*, 13148.
(6) (a) Marcus, R. A. *J. Chem. Phys.* **1956**, *24*, 966. (b) *Rev. Mod. Phys.* **1993**, *65*, 599. (c) Marcus, R. A.; Sutin, N. *Biochim. Biophys. Acta* **1985**, *811*, 265.
(7) Bixon, M.; Jortner, J.; Michel-Beyerle, M. E. *Biochim. Biophys. Acta* **1991**, *1056*, 301; *Chem. Phys.* **1995**, *197*, 389.
(8) Deisenhofer, J.; Epp, O.; Miki, K.; Huber, R.; Michel, H. *J. Mol. Biol.* **1984**, *180*, 385.
(9) (a) Wasielewski, M. R. *Chem. Rev.* **1992**, *92*, 345. (b) Wasielewski, M. R.; Johnson, D. G.; Svec, W. A.; Kersey, K. M.; Cragg, D. E.; Minsek, D. W. *Photochemical Energy Conversion*; Norris, J., Meisel, D., Eds.; Elsevier: Amsterdam, 1989; p 135. (c) Wasielewski, M. R.; Niemczyk, M. P.; Johnson, D. G.; Svec, W. A.; Minsek, D. W. *Tetrahedron* **1989**, *45*, 4785.
(10) Johnson, D. G.; Niemczyk, M. P.; Minsek, D. W.; Wiederrecht, G. P.; Svec, W. A.; Gaines, G. L., III; Wasielevski, M. R. *J. Am. Chem. Soc.* **1993**, *115*, 5692.
(11) Davis, W.; Wasielewski, M.; Ratner, M.; Mujica, V.; Nitzan, A. *J. Phys. Chem.* **1997**, *101*, 6158.
(12) Scourtis, S. S.; Mukamel, S. *Chem. Phys.* **1995**, *197*, 367.
(13) Schreiber, M.; Fuchs, C.; Scholz, R. *J. Lumin.* **1998**, *76* and *77*, 482.
(14) McConnel, H. M. *J. Chem. Phys.* **1961**, *35*, 508.
(15) Kosloff, R.; Ratner, M. A. *Isr. J. Chem.* **1990**, *30*, 45.
(16) Rempel, U.; von Maltzan, B.; von Borczyskowski, C. *Chem. Phys. Lett.* **1995**, *245*, 253.
(17) (a) Zenkevich, E. I.; Knyukshto, V. N.; Shulga, A. M.; Kuzmitsky, V. A.; Gael, V. I.; Levinson, E. G.; Mironov, A. F. *J. Lumin.* **1997**, *75*, 229. (b) Zenkevich, E. I.; Shulga, A. M.; Bachilo, S. M.; Rempel, U.; von Richthofen, J.; von Borczyskowski, C. *J. Lumin.* **1998**, *76* and *77*, 354. (c) Chernook, A.; Rempel, U.; von Borczyskowski, C.; Shulga, A. M.; Zenkevich, E. I. *Chem. Phys. Lett.* **1996**, *254*, 229. (d) *J. Phys. Chem.* **1996**, *100*, 1918. (e) *Ber. Bunsen-Ges. Phys. Chem.* **1996**, *100*, 2065.
(18) Burstein, A. I.; Georgievskii, Y. *J. Chem. Phys.* **1994**, *100*, 7319.
(19) (a) Sumi, H.; Kakitani, T. *Chem. Phys. Lett.* **1996**, *252*, 85. (b) Sumi, H. *Electroanal. J. Chem.* **1997**, *438*, 11.
(20) Paulson, B.; Pramod, K.; Eaton, P.; Closs, G. L.; Miller, J. R. *J. Chem. Phys.* **1993**, *97*, 13042.
(21) Hush, N. S. *Coord. Chem. Rev.* **1985**, *64*, 135.
(22) (a) Langen, R.; Chang, I.; Germanas, J. P.; Richards, J. H.; Winkler, J. R.; Gray, H. B. *Science* **1995**, *268*, 1733. (b) Murphy, C. J.; Arkin, M. R.; Jenkins, Y.; Ghatlia, N. D.; Bossman, S. H.; Turro, N. J.; Barton, J. K. *Science* **1993**, *262*, 1025.
(23) (a) Mujica, V.; Kemp, M.; Ratner, M. A. *J. Chem. Phys.* **1994**, *101*, 6849. (b) **1994**, *101*, 6856. (c) Kemp, M.; Mujica, V.; Ratner, M. A. *J. Chem. Phys.* **1994**, *101*, 5172. (d) Mujica, V.; Kemp, M.; Roitberg, A.; Ratner, M. A. *J. Chem. Phys.* **1996**, *104*, 7296. (e) Samanta, M. P.; Tian, W.; Datta, S.; Henderson, J. I.; Kubiak, C. P. *Phys. Rev. B* **1996**, *53*, R7626.
(24) (a) Ratner, M. A. *J. Phys. Chem.* **1990**, *94*, 4877. (b) Miller, R. J.; Beitz, J. V. *J. Chem. Phys.* **1981**, *74*, 6749.
(25) (a) Evenson, J. W.; Karplus, M. *J. Chem. Phys.* **1992**, *96*, 5272. (b) *Science*, **1993**, *262*, 1247.
(26) Pollard, W. T.; Felts, A. K.; Friesner, R. A. *Adv. Chem. Phys.* **1996**, *93*, 77.
(27) Davis, W. B.; Svec, W. A.; Ratner, M. A.; Wasielewski, M. R. *Nature* **1998**, *396*, 60.
(28) Cave, R.; Newton, M. D. *Chem. Phys. Lett.* **1996**, *249*, 15.
(29) Bixon, M.; Jortner, J. *J. Chem. Phys.* **1997**, *107*, 5154.
(30) Weiss, U. *Quantum Dissipative Systems*; World Scientific: Singapore, 1999.
(31) (a) Loudon, R. *The Quantum Theory of Light*; Clarendon: Oxford, 1973. (b) Klauder, J. R.; Sudarshan, E. C. G. *Fundamentals of Quantum Optics*; Benjamin: New York, 1968.

(32) (a) Egger, R.; Mak, C. H.; Weiss, U. *Phys. Rev. E* **1994**, *50*, R655. (b) Mak, C. H.; Egger, R. *Chem. Phys. Lett.* **1995**, *238*, 149. (c) Makri, N.; Sim, E.; Makarov, E.; Topaler, M. *Proc. Natl. Acad. Sci. U.S.A.* **1996**, *93*, 3926. (d) Sim, E.; Makri, N. *J. Phys. Chem. B* **1997**, *101*, 5446.

(33) Felts, A. K.; Pollard, W. T.; Friesner, R. A. *J. Phys. Chem.* **1995**, *99*, 2929.

(34) Lin, S. H.; Hayashi, M.; Suzuki, S.; Gu, X.; Xiao, W.; Sugawara, M. *Chem. Phys.* **1995**, *197*, 435.

(35) Kühn, O.; Rupasov, V.; Mukamel, S. *J. Chem. Phys.* **1996**, *104*, 5821.

(36) Guo, H.; Liu, L.; Lao, K. *Chem. Phys. Lett.* **1994**, *218*, 212.

(37) Fano, U. *Rev. Mod. Phys.* **1957**, *29*, 74.

(38) Blum, K. *Density Matrix Theory and Applications*; Plenum: New York, 1996.

(39) (a) Redfield, A. G.; *IBM J. Res. Dev.* **1957**, *1*, 19. (b) *Adv. Magn. Reson.* **1965**, *1*, 1.

(40) May, V.; Schreiber, M. *Phys. Rev. A* **1992**, *45*, 2868.

(41) Kühn, O.; May, V.; Schreiber, M. *J. Chem. Phys.* **1994**, *101*, 10404.

(42) (a) Jean, J. M.; Friesner, R. A.; Fleming, G. R. *J. Chem. Phys.* **1992**, *96*, 5827. (b) Pollard, W. T.; Friesner, R. A. *J. Chem. Phys.* **1994**, *100*, 5054. (c) Jean, J. M.; Fleming, G. R. *J. Chem. Phys.* **1995**, *103*, 2092. (d) Jean, J. M. *J. Chem. Phys.* **1996**, *104*, 5638.

(43) (a) Nitzan, A. *Chem. Phys.* **1979**, *41*, 163. (b) Kosloff, R.; Rice, S. A. *J. Chem. Phys.* **1980**, *72*, 4591.

(44) Kosloff, R.; Ratner, M. A.; Davis, W. B. *J. Chem. Phys.* **1997**, *106*, 7036.

(45) Schreiber, M.; Kilin, D. *Proceedings of the 2nd International Conference on Excitonic Processes in Condensed Matter*; M. Schreiber, Ed.; Dresden University Press: Dresden, 1996; p 331.

(46) Davis, W. B.; Wasielewski, M. R.; Kosloff, R.; Ratner, M. A. *J. Phys. Chem. A* **1998**, *102*, 9360.

(47) (a) Čápek, V. *Z. Phys. B* **1985**, *60*, 101. (b) Čápek, V.; Szöcs, V. *Phys. Status Solidi B* **1985**, *131*, 667.

(48) Silinsh, E. A.; Čápek, V. *Organic Molecular Crystals*; American Institute of Physics: New York, 1994.

(49) Kenkre, V.; Reineker, P. *Exciton Dynamics in Molecular Crystals and Aggregates*; Springer: Berlin, 1982.

(50) Haken, H.; Reineker, P. *Z. Phys.* **1972**, *249*, 253.

(51) Weitz, D. A.; Garoff, S.; Gersten, J. I.; Nitzan, A. *J. Chem. Phys.* **1983**, *78*, 5324.

(52) Kilin, D.; Schreiber, M. *J. Lumin.* **1998**, *76* and *77*, 433.

(53) Gouterman, M. *J. Mol. Spectrosc.* **1961**, *6*, 138.

(54) Schreiber, M.; Kilin, D.; Kleinekathöfer, U. *J. Lumin.* **1999**, *83* and *84*, 235.

(55) Fraser, D. D.; Bolton, J. R. *J. Phys. Chem.* **1994**, *98*, 1626.

(56) (a) Agranovich, V. M.; Galanin, M. D. *Electronic Excitation Energy Transfer in Condensed Matter*; North-Holland: Amsterdam, 1982. (b) Landau, L. D.; Lifshitz, E. M. *Lehrbuch der Theoretischen Physik, Band VIII*; Akademie-Verlag: Berlin 1985.

(57) Georgievskii, Y.; Hsu, C.-P.; Marcus, R. A. *J. Chem. Phys.* **1999**, *110*, 5307.

(58) Christiansen, O.; Mikkelsen, K. *J. Chem. Phys.* **1999**, *110*, 8348.

(59) Feynman, R. P. *The Feynman Lectures on Physics Vol. III*; Addison-Wesley: Reading, 1963.

(60) Böttcher, C. J. F. *Theory of Electric Polarization*; Elsevier: Amsterdam, 1973; Vol. 1.

(61) Karelson, M.; Diercksen, G. H. F. In *Problem Solving in Computational Molecular Science: Molecules in Different Environments*; Wilson, S., Diercksen, G. H. F., Eds.; Kluwer: Dordrecht, 1997; p 195.

(62) Yosida, K. *Theory of Magnetism*; Springer: Berlin, 1996.

(63) Tyablikov, S. V. *Methods of the Quantum Theory of Magnetism*; Plenum: New York, 1967.

(64) Apanasevich, P. A.; Kilin, S. Ya.; Nizovtsev, A. P.; Onishchenko, N. S. *J. Opt. Soc. Am. B* **1986**, *3*, 587.

(65) (a) Yoon, B.; Deutch, J. M.; Freed, J. H. *J. Chem. Phys.* **1975**, *362*, 4687. (b) Isihara, A. *Statistical Physics*; Academic Press: New York, 1971.

(66) Mataga, N.; Kaifu, Y.; Koizumi, M. *Bull. Chem. Soc. Jpn.* **1956**, *29*, 465.

(67) Rempel, U. Ph.D. Thesis; Eveie Universität, Berlin, 1993.

(68) One can compare these energies with the energies of the same levels of H−chlorine−Zn−porphyrin−quinone in solution of butonitrile,[10] namely $E_{D}{*}_{BA} = 1.85$, $E_{D^+B^-A} = 3.05$, $E_{DB}{*}_{A} = 2.12$, $E_{DB^+A^-} = 2.15$, $E_{D^+BA^-} = 1.47$ eV. The present modeling can be applied to this very similar molecular aggregate using the same approximations.

(69) Cichos, F. Ph.D. Thesis; Technische Universität, Chemnitz, 1998.

(70) Domcke, W.; Stock, G. *Adv. Chem. Phys.* **1997**, *100*, 1.